Title	Isolation of the simplest hydrated acid
Author(s)	Zhang, Rui; Murata, Michihisa; Wakamiya, Atsushi; Shimoaka, Takafumi; Hasegawa, Takeshi; Murata, Yasujiro
Citation	Science Advances (2017), 3(4)
Issue Date	2017-04-21
URL	http://hdl.handle.net/2433/220440
Right	Copyright © 2017, The Authors This is an open-access article distributed under the terms of the Creative Commons Attribution-NonCommercial license, which permits use, distribution, and reproduction in any medium, so long as the resultant use is not for commercial advantage and provided the original work is properly cited.
Type	Journal Article
Textversion	publisher

CHEMISTRY

Isolation of the simplest hydrated acid

Rui Zhang, Michihisa Murata, Atsushi Wakamiya, Takafumi Shimoaka, Takeshi Hasegawa, Yasujiro Murata*

Dissociation of an acid molecule in aqueous media is one of the most fundamental solvation processes but its details remain poorly understood at the distinct molecular level. Conducting high-pressure treatments of an open-cage fullerene C_{70} derivative with hydrogen fluoride (HF) in the presence of H_2O, we achieved an unprecedented encapsulation of H_2O·HF and H_2O. Restoration of the opening yielded the endohedral C_{70}s, that is, (H_2O·HF)@C_{70}, H_2O@C_{70}, and HF@C_{70} in macroscopic scales. Putting an H_2O·HF complex into the fullerene cage was a crucial step, and it would proceed by the synergistic effects of "pushing from outside" and "pulling from inside." The structure of the H_2O·HF was unambiguously determined by single crystal x-ray diffraction analysis. The nuclear magnetic resonance measurements revealed the formation of a hydrogen bond between the H_2O and HF molecules without proton transfer even at 140°C.

INTRODUCTION

One of the most important chemical processes is dissociation of a Brønsted acid in aqueous media accompanied by proton transfer from the acid to H_2O molecules and solvation of the charged fragments (*1*). This fundamental event plays a key role in myriad chemical reactions and biological phenomena. However, the detailed mechanism of acid dissociation (*2*, *3*) and the nature of protons in an aqueous environment (*4*, *5*) are rather complex, and still remain to be revealed at the distinct molecular level. Hydrogen fluoride (HF) is the smallest acid and has been studied well, mostly in the gas phase, both theoretically and experimentally (*6*). One extensively discussed issue on HF is the minimum number of H_2O molecules that is necessary to solvate an HF molecule resulting in the formation of the solvent-shared ion pair $[H_3O^+(H_2O)_nF^-]$ (*3*, *7*, *8*). However, the central obstacle to resolution of this subject includes the difficulty of preparation of any of the possible HF·$(H_2O)_n$ complexes in a pure form with definite components. This is because the high reactivity of HF and the strong hydrogen bond affinity of H_2O often result in the formation of many types of oligomers, which are in equilibrium with others, rendering their separation and isolation almost impossible (*9*). To understand this fundamental process, it is highly desirable to construct an ideal system that can elucidate the intrinsic nature of the hydrated HF molecule.

To isolate reactive chemical species, the compounds should be located in an inert atmosphere, preventing interaction and/or reaction from the outer environments. These subnano-sized environments can be found inside fullerenes, which are spherical carbon clusters having a hollow cavity. Very reactive chemical species such as metal ions (*10*, *11*), metal clusters (*12*), and a nitrogen atom (*13*) have thus far been encapsulated inside fullerenes. These well-defined supramolecular systems have provided opportunities to study the physical and chemical properties of the encapsulated species at the molecular scale and to use them as functional materials (*14*). However, selectivity in encapsulated species in addition to fullerene cages are difficult to control because of the reliance of most production methods on harsh conditions (*12*, *14*). In contrast, the "molecular surgery" approach can produce molecule-encapsulating fullerenes with almost-perfect selectivities under mild conditions in solution (*15*). Using this method, endohedral C_{60} encapsulating a single molecule of H_2 (*16*), He (*17*), H_2O (*18*), and HF (*19*) was synthesized.

Molecular surgery can also be applied to fullerene C_{70} despite difficulties in characterization of products due to low symmetry. Reflecting the larger inner space in C_{70} compared to C_{60} (*20*, *21*), two small molecules were introduced inside open-cage C_{70} derivatives to afford the corresponding doubly encapsulating endohedral C_{70}s after restoration of the cage, that is, $(H_2)_2$@C_{70} (*22*) and $(H_2O)_2$@C_{70} (*23*), respectively. Previously, we reported two open-cage C_{70} derivatives, **α-13mem** (*24*) and **β-13mem** (Fig. 1A) (*23*), both having a 13-membered ring opening with the same functional groups. These compounds were synthesized by a three-step reaction starting from the addition of a pyridazine derivative to the α- and β-bonds of C_{70}, with total yields of 22 and 2%, respectively. Both openings were enlarged in situ into the 16-membered ring as their C_{60} analog (*18*). The opening of **α-16mem** is smaller than that of **β-16mem**, evidenced by the fact that only a trace amount of H_2O was introduced inside **α-16mem**, whereas an H_2O molecule was entrapped almost quantitatively inside **β-16mem**. Density functional theory (DFT) calculations also supported the smaller size of **α-16mem** (*23*). Taking advantage of the efficient synthetic yield of **α-13mem**, we envisioned that **α-13mem** would be more suitable as a starting material for novel endohedral C_{70}s. Because the size of HF is smaller than that of H_2O (*25*), we studied encapsulation of HF into **α-13mem** with initial intention to synthesize HF@C_{70}. Here, we report facile synthesis of HF@C_{70}, as well as unprecedented formation of (H_2O·HF)@C_{70} and H_2O@C_{70}, using **α-13mem** as a key compound despite the small size of the opening for the insertion of H_2O.

As shown in Fig. 1B, after optimization of the conditions (vide infra), the high-pressure treatment of **α-13mem** in the presence of 0.5 equivalence of 70% (w/w) HF in pyridine (HF-Py) (*26*) and a trace amount of water was conducted in chlorobenzene under 9000 atm at 120°C for 18 hours to afford guest-encapsulating **α-13mem** (G@**α-13mem**; G = HF, H_2O·HF, and H_2O) in 40% isolated yield after purification with column chromatography. The filling factors of the guests inside **α-13mem** were determined by the proton nuclear magnetic resonance (^{1}H NMR) analysis: 32% HF@**α-13mem**, 11% (H_2O·HF)@**α-13mem**, 27% H_2O@**α-13mem**, and 30% empty **α-13mem**, respectively. After collecting the products from several batches, closing of G@**α-13mem** via two-step reactions, without considerable loss of the encapsulated species, gave the corresponding endohedral C_{70}s, that is, expected

Institute for Chemical Research, Kyoto University, Uji, Kyoto 611-0011, Japan.
*Corresponding author. Email: yasujiro@scl.kyoto-u.ac.jp

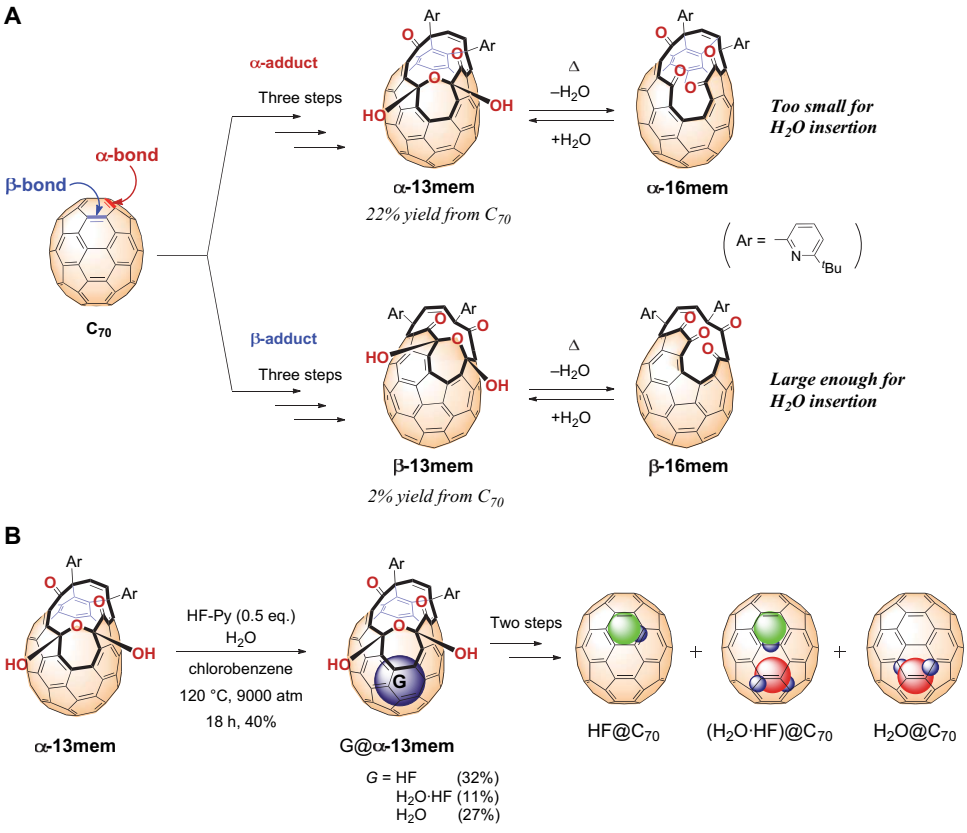

Fig. 1. Molecular surgery for the synthesis of endohedral fullerene C_{70}s. (**A**) Two open-cage C_{70} derivatives **α-13mem** and **β-13mem** obtained from the initial addition of a pyridazine derivative to the **α**-bond and β-bond of C_{70} followed by stepwise cleavages of the C=C double bonds. The openings of **α-13mem** and **β-13mem** are enlarged in situ by dehydration to afford **α-16mem** and β-**16mem**. The opening size of **α-16mem** is too small for H_2O insertion, whereas that of β-**16mem** is large enough. (**B**) Insertion of the guest molecules (G = HF, H_2O·HF, and H_2O) into **α-13mem** and synthesis of HF@C_{70}, (H_2O·HF)@C_{70}, and H_2O@C_{70} by closure of the opening via two-step reactions.

HF@C_{70}, and unprecedented (H_2O·HF)@C_{70} and H_2O@C_{70} (figs. S8 to S15).

We confirmed that HF encapsulation into **α-16mem** did not take place in chlorobenzene under ambient pressure at 110°C, in contrast to the case for the open-cage C_{60} (*25*). Thus, the high-pressure conditions were found to be critical, where the guest species are forced to be "pushed from outside" of the opening of **α-16mem**. The experimental conditions and results are summarized in Table 1. Upon checking the time dependence (entries 1 to 4), the filling factor of HF appeared to almost reach a plateau after 14 hours, whereas that of H_2O·HF increased slowly and that of H_2O was developed rapidly at around 14 hours. These observations suggested stepwise formation of G@**α-16mem**, that is, HF@**α-16mem** followed by (H_2O·HF)@**α-16mem** and then H_2O@**α-16mem**. To prevent a high degree of decomposition of the starting materials and the products, a reduced amount of HF-Py at slightly higher temperature gave the better chemical yield of G@**α-13mem** (entry 5). As described previously by Zhang *et al.* (*23*, *24*), H_2O encapsulation did not occur in the absence of HF (entry 6), showing only that pushing from outside was not an effective method of inserting H_2O inside **α-16mem**. Among the products obtained from entries 1 to 5, $(HF)_2$@**α-13mem** and $(H_2O)_2$@**α-13mem** were not detected.

Our experiments considered the insertion mechanisms of HF, H_2O·HF, and H_2O (as shown in Fig. 2). Because the size of the opening of **α-16mem**, which was generated in situ from **α-13mem** by eliminating a water molecule from the bis(hemiketal) moiety, is not large enough for water to pass through, insertion of a smaller HF initially takes place by pushing from outside to give molecular complex **A**. In earlier work, Gan *et al.* (*27*) reported that encapsulated H_2O inside an open-cage C_{60} was pulled out by attractive interaction with fluorine atom being present outside the opening, resulting in the release of the H_2O. Taking into consideration the similar attractive interaction of the encapsulated HF and the H_2O near the opening, the H_2O should be introduced into **α-16mem** by the assist of "pulling from inside," shown as **B**, to yield **C**. Then, positional exchange of the lower HF and the upper H_2O occurs to afford **D**. DFT calculations at the M06-2X/6-31G(d) level showed that the required energy for the positional exchange of the HF and H_2O in **C** is 20.8 kcal/mol (tables S3 to S5), which should be possible to occur under the applied conditions. Finally, the resulting HF near the opening escapes to form **E**. During the cooling process, addition of a water molecule regenerates the **α-13mem** cage to furnish G@**α-13mem**.

Because of the complexities in the structures of H_2O clusters and hydrated HF, it is very difficult to evaluate energy profiles including **A**, **B**, **D**, and **E** by DFT studies. In the case of the gas-phase stabilization energy calculated at the MP2/6-311++G(3pd,3df) level, H_2O·HF gains more energy (7.3 kcal/mol) than HF dimer (3.9 kcal/mol) and H_2O dimer (3.8 kcal/mol) (tables S8 to S15). This stability is considered to play an important role for the formation of **C.** However, we needed to study another possibility that the presence of an acid would change

the solvated structures of HF and H_2O before encapsulation to result in facile encapsulation of H_2O. Although a high-pressure treatment in the presence of HCl-Py, instead of HF-Py, under the same conditions was conducted, the resulting products obtained in 64% isolated yield were found to contain only a small amount of H_2O@**α-13mem** (1.8% filling factor). These results strongly support the hypothesis that both pushing and pulling effects are necessary to achieve encapsulation of H_2O·HF inside **α-13mem** in a remarkably high yield compared with the doubly encapsulating C_{70}s reported so far (*22*, *23*).

After closure of the openings (Fig. 1B), the high-performance liquid chromatography (HPLC) analysis of the products displayed three peaks corresponding to empty C_{70}, a mixture of HF@C_{70} and H_2O@C_{70}, and (H_2O·HF)@C_{70} (as shown in Fig. 3A). The mono-encapsulating HF@C_{70} and H_2O@C_{70} appeared at almost the same retention time regardless of the encapsulated species. In contrast, facile separation of (H_2O·HF)@C_{70} as a pure form was achieved in a preparative scale, showing clear differences caused by the double encapsulation. By the atmospheric pressure chemical ionization mass analysis (APCI MS), we detected (HF)$_2$@C_{70} before elution of (H_2O·HF)@C_{70}, albeit in only a trace amount (fig. S16).

The ^{1}H NMR analysis is a powerful tool to study the structure and dynamics of the isolated H_2O·HF. As shown in Fig. 3B, a signal of the singly encapsulated H_2O at −27.1 parts per million (ppm) [500 MHz; $CDCl_3/CS_2$ (1:1), 25°C] coincides with that of our previous report for H_2O@C_{70} synthesized from different synthetic routes (*23*), showing strong shielding effects due to C_{70} cage (*22*, *23*). A doublet corresponding to the singly encapsulated HF was observed at −25.0 ppm with a coupling constant J_{HF} = 507 Hz, whose value is almost the same as that of HF@C_{60} (*19*). The ^{1}H NMR of (H_2O·HF)@C_{70} displayed a singlet at −25.3 ppm corresponding to the H_2O in addition to a doublet at −17.5 ppm corresponding to the HF. It is noteworthy that both chemical shifts are downfield-shifted compared with those of H_2O@C_{70} and HF@C_{70}, indicating more positive charges on the protons due to the formation of a hydrogen bond. The shifted value for the HF (Δδ +7.5) is larger than that of the H_2O (Δδ +1.8), demonstrating that this molecular complex adopts the structure H_2O·HF, in which the oxygen works as a hydrogen bond acceptor, rather than HF·H_2O, in which the fluorine works as the acceptor. In addition, the smaller value of the coupling constant J_{HF} = 443 Hz also supports the structure H_2O·HF, the value being close to those of HF in diethyl ether and dimethyl sulfoxide solutions, J_{HF} = 464 and 410 Hz, respectively (*28*). Hence, we concluded that this is the simplest hydrated acid. Upon heating the solution in *ortho*-dichlorobenzene-d_4 (ODCB-d_4), no change in the spectral shape was observed even at 140°C, revealing that no proton transfer takes place between the H_2O and HF on the NMR time scale.

The structure of (H_2O·HF)@C_{70} was unambiguously determined by the single-crystal x-ray diffraction analysis for the crystals containing nickel(II) octaethylporphyrin and solvent molecules, with almost the same unit cell constants as those of empty C_{70} (*29*) and H_2O@C_{70} (*23*). As shown in Fig. 3D, the O and F atoms of the H_2O·HF were observed inside the C_{70} located on the porphyrin. It is the first example of the x-ray structure for doubly encapsulating C_{70}. Here, in contrast to

Table 1. Encapsulation of HF, H_2O·HF, and H_2O inside α-13mem under the high-pressure conditions of 9000 atm in the chlorobenzene solution.

Entry	HF-Py (eq.)	Temperature (°C)	Time (hours)	Yield (%)*	Filling factor (%)†		
					HF	H_2O·HF	H_2O
1	1	110	3	34	1.8	0.9	1.2
2	1	110	6	23	24	15	5
3	1	110	14	29	32	16	22
4	1	110	18	20	32	20	33
5	0.5	120	18	40	32	11	27
6	0	120	18	87	0	0	4.4

*Isolated yields of the sum of recovered **α-13mem** and G@**α-13mem** (G = HF, H_2O·HF, and H_2O) after purification with a column chromatography on silica gel. †The filling factors were determined by comparison of the integral values of the encapsulated species (δ −18.2 ppm for HF, −15.6 ppm for H_2O·HF, and −11.8 ppm for H_2O) with that of the organic addends (δ 6.7 ppm for the olefinic proton at the opening) in the ^{1}H NMR [500 MHz; $CDCl_3/CS_2$ (1:1)] spectra.

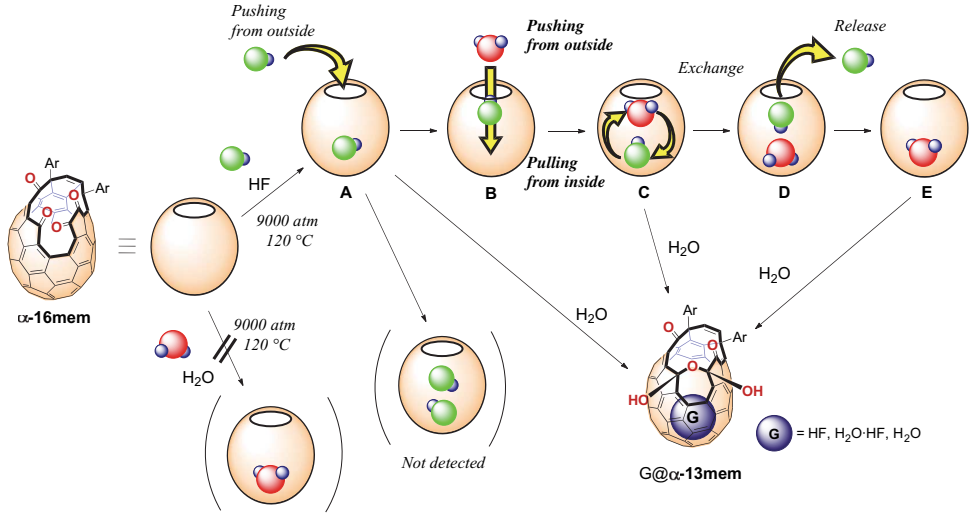

Fig. 2. Insertion mechanism of HF, H_2O·HF, and H_2O into α-16mem with the synergestic effects of pushing from outside by high-pressure conditions and pulling from inside by attractive interaction of HF with the outer H_2O.

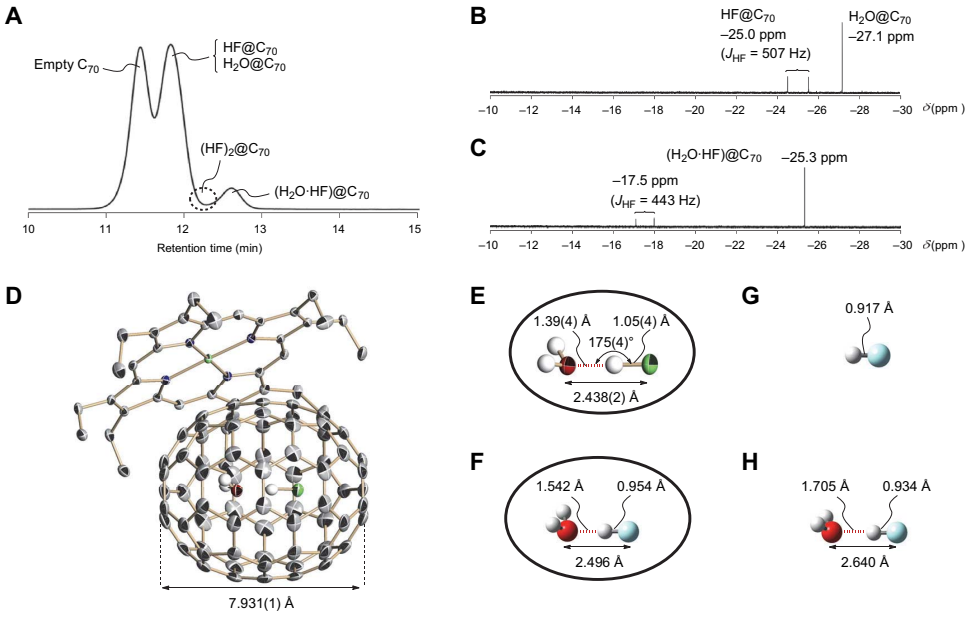

Fig. 3. Properties of $(H_2O{\cdot}HF)$@C_{70}. (**A**) HPLC trace of reaction products after the complete closure of the opening. The HPLC was equipped with the Cosmosil Buckyprep column (4.6φ × 250 mm) eluted with toluene at 50°C. ^{1}H NMR (500 MHz) spectra in $CDCl_3/CS_2$ (1:1) at 25°C of (**B**) a mixture of HF@C_{70} and H_2O@C_{70}, and (**C**) pure $(H_2O{\cdot}HF)$@C_{70}. (**D**) Single crystal x-ray structure of $(H_2O{\cdot}HF)$@C_{70} with thermal ellipsoids at the 50% level, with cocrystalized nickel(II)octaethylporphyrin. Solvent molecules and hydrogen atoms were omitted for clarity. (**E**) Detailed x-ray structure of the encapsulated $H_2O{\cdot}HF$ complex. The H atom between O and F was refined, whereas the other two H atoms were geometrically fixed. (**F**) Calculated structure of $(H_2O{\cdot}HF)$@C_{70} at the ONIOM-(MP2/6-311++G(3df,3pd):M06-2X/6-31G(d)). Only the encapsulated species were shown. Calculated structures at the MP2/6-311++G(3df,3pd) of (**G**) a free HF and (**H**) a free $H_2O{\cdot}HF$.

the x-ray structure of H_2O@C_{70} with dynamic disorder on the position of the O, the O and F in this study did not show any dynamic or positional disorder, demonstrating the perfect alignment of the $H_2O{\cdot}HF$. Reflecting its dense encapsulation, the averaged longer axis of the C_{70} cage [7.931(1) Å] was elongated by 0.20% compared with that of H_2O@C_{70} [7.915(1) Å]. The distance between the O and F was 2.438(2) Å (Fig. 3E). It should be mentioned that the position of H between O and F was experimentally determined and refined, showing a distance of 1.39(4) and 1.05(4) Å, respectively. Thus, $H_2O{\cdot}HF$ was found to adopt such structure as the proton of HF forms a liner hydrogen bond to the oxygen of H_2O, which is in good agreement with the ^{1}H NMR results.

To obtain deeper insights, the structure of $(H_2O{\cdot}HF)$@C_{70} was optimized at the ONIOM (our own n-layered integrated molecular orbital and molecular mechanics)-(MP2/6-311++G(3pd,3df):M06-2X/6-31G(d)) level (Fig. 3F). The calculated structure was found to reproduce well the x-ray structure, showing a distance of 2.496 Å between O and F as well as 0.15% elongation of the cage. Then, an HF molecule and a molecular complex $H_2O{\cdot}HF$, in free forms in a gas phase, were calculated at the MP2/6-311++G(3pd,3df) level (Fig. 3, G and H). Comparison of the calculated structures of $(H_2O{\cdot}HF)$@C_{70} with free $H_2O{\cdot}HF$ demonstrated that the O–F (2.496 Å) and O–H (1.542 Å) distances are shorter by 5.5 and 9.6%, respectively, whereas the H–F bond is longer by 2.1%. These data supported the hypothesis that a contact ion character described as $H_3O^+{\cdot}F^-$ slightly appears by compression of the H_2O and HF inside the limited space. The positional exchange of the H_2O and HF was not detected at room temperature because the ^{13}C NMR of $(H_2O{\cdot}HF)$@C_{70} displayed nine signals due to its C_{5v} symmetry (fig. S14), in contrast to the averaged D_{5h} symmetry of H_2O@C_{70} and HF@C_{70} with dynamic motion of the encapsulated species.

The molecular complex $H_2O{\cdot}HF$ should have a polarity, which could affect the properties of the outer C_{70} cage. In the ^{13}C NMR spectra, the chemical shifts of the cage carbons near the H_2O are smaller than those near the HF, indicating the polarity of $(H_2O{\cdot}HF)$@C_{70}, which was shown by the gauge-independent atomic orbital (GIAO) calculations (fig. S17). However, this polarity was not obvious on reduction potentials determined by cyclic voltammetry (CV) in ODCB, the first reduction potentials for $(H_2O{\cdot}HF)$@C_{70} and empty C_{70} being −1.04 and −1.06 V versus a ferrocene/ferrocenium couple (fig. S18). The ultraviolet-visible (UV-vis) absorption in toluene is almost superimposable with that of empty C_{70} (fig. S19). The infrared (IR) bands for the HO–H and F–H bonds were not observed, probably due to the shielding effects of the cage, which was the same for H_2O@C_{60} (*18*), HF@C_{60} (*19*), and H_2O@C_{70} (*23*). However, interesting suppression of the characteristic IR bands of C_{70} was observed for HF@C_{70} and $(H_2O{\cdot}HF)$@C_{70} (fig. S20).

In summary, the simplest hydrated HF was isolated in a confined subnano space by the use of molecular surgical methods. Compared with the doubly encapsulating C_{70}s reported so far, a high efficiency of the encapsulation was achieved because of the synergetic effects of pushing from outside by the high-pressure conditions and pulling from inside with an attractive interaction of the encapsulated HF with the outer H_2O, which was supported by the stepwise formation of HF@C_{70}, followed by $(H_2O{\cdot}HF)$@C_{70} and then H_2O@C_{70}. The NMR studies revealed the rigid structure of the $H_2O{\cdot}HF$ without hydrogen exchange. The single crystal x-ray analysis and theoretical calculations showed the closer contact of the oxygen with the hydrogen of HF compared with that of free $H_2O{\cdot}HF$.

MATERIALS AND METHODS

General

The ^{1}H, ^{13}C, and ^{19}F NMR measurements were performed with the JEOL JNM-ECA 500 and JNE-ECA 600 instruments. The NMR chemical

shifts were reported in parts per million with reference to residual protons, carbons, and fluorine of $CDCl_3$ (δ 7.26 ppm in ^{1}H NMR, δ 77.0 ppm in ^{13}C NMR), tetrahydrofuran (THF-d_8) (δ 67.57 ppm in ^{13}C NMR), and hexafluorobenzene (C_6F_6) (δ 164.90 ppm in ^{19}F NMR). The APCI MS spectra were measured on a Bruker micrOTOF-Q II. High-pressure experiments were conducted by using the Hikari Koatsu high-pressure apparatus HR15-B3. The HPLC was performed with a Cosmosil Buckyprep column (4.6φ × 250 mm) for analytical purpose and the same columns (two directly connected columns; 20φ × 250 mm) for preparative purpose. CV was conducted in an ALS Electrochemical Analyzer Model 620C using a three-electrode cell with a glassy carbon working electrode, a platinum wire counter electrode, and a Ag/0.01 M $AgNO_3$ reference electrode. UV-vis spectra were recorded with a Shimadzu UV-3150 spectrometer. The IR spectra were collected by using a Thermo Fisher Scientific Magna 550 FT-IR spectrometer equipped with a Harrick Scientific VRA reflection attachment (*30*). The detector was a liquid nitrogen–cooled mercury-cadmium-telluride detector with a modulation frequency of 60 kHz. The number of accumulation was 1000, and the wavenumber resolution was 4 cm^{-1}. Fullerene C_{70} was purchased from SES Research Co. Triisopropyl phosphite was purchased from Tokyo Chemical Industry Co. Ltd. Hydrogen fluoride pyridine was purchased from Sigma-Aldrich. The open-cage C_{70} derivative **α-13mem** was prepared according to a previous report (*24*).

Computational methods

All calculations were conducted with Gaussian 09 packages (*31*). The structures were optimized at the M06-2X/6-31G(d), MP2/6-311++G(3df,3pd), and ONIOM-(MP2/6-311++G(3df,3pd):M06-2X/6-31G(d)) levels without any symmetry assumptions (*32*). For the ONIOM method, the MP2 method was applied for the endohedral species and the M06-2X method was used for the fullerene cage. All structures including the stationary states and the transition states were confirmed by the frequency calculations at the same level. The calculated ^{1}H NMR and ^{13}C NMR chemical shifts were obtained at the GIAO-B3LYP/6-311G(d,p) level using the optimized structures at the ONIOM or M06-2X methods with a reference of tetramethylsilane calculated at the GIAO-B3LYP/6-311G(d,p)//M06-2X/6-31G(d) level. The isotropic chemical shifts were calculated for protons (32.3196 ppm) and carbons (185.7282 ppm).

SUPPLEMENTARY MATERIALS

Supplementary material for this article is available at http://advances.sciencemag.org/cgi/content/full/3/4/e1602833/DC1

Supplementary Text

fig. S1. ^{1}H NMR [500 MHz; $CDCl_3/CS_2$ (1:1)] spectrum of a mixture of HF@**α-13mem**, (H_2O·HF)@**α-13mem**, H_2O@**α-13mem**, and empty **α-13mem**.

fig. S2. ^{13}C NMR (151 MHz; THF-d_8) spectrum of a mixture of HF@**α-13mem**, (H_2O·HF)@**α-13mem**, H_2O@**α-13mem**, and empty **α-13mem**.

fig. S3. ^{19}F NMR [470 MHz; $CDCl_3/CS_2$ (1:1)] spectrum of a mixture of HF@**α-13mem**, (H_2O·HF)@**α-13mem**, H_2O@**α-13mem**, and empty **α-13mem**.

fig. S4. ^{1}H NMR [500 MHz; $CDCl_3/CS_2$ (1:1)] spectrum of a mixture of HF@**α-13mem**, (H_2O·HF)@**α-13mem**, H_2O@**α-13mem**, and empty **α-13mem** obtained under the optimized conditions (Table 1, entry 5).

fig. S5. ^{1}H NMR (500 MHz; $CDCl_3$) spectrum of a mixture of HF@**α-8mem**, (H_2O·HF)@**α-8mem**, H_2O@**α-8mem**, and empty **α-8mem**.

fig. S6. ^{13}C NMR (151 MHz; $CDCl_3$) spectrum of a mixture of HF@**α-8mem**, (H_2O·HF)@**α-8mem**, H_2O@**α-8mem**, and empty **α-8mem**.

fig. S7. ^{19}F NMR (470 MHz; $CDCl_3$) spectrum of a mixture of HF@**α-8mem**, (H_2O·HF)@**α-8mem**, H_2O@**α-8mem**, and empty **α-8mem**.

fig. S8. ^{1}H NMR [500 MHz; $CDCl_3/CS_2$ (1:1)] spectrum of a mixture of HF@C_{70} and H_2O@C_{70} (1:1).

fig. S9. ^{19}F NMR [470 MHz; $CDCl_3/CS_2$ (1:1)] spectrum of a mixture of HF@C_{70} and H_2O@C_{70} (1:1).

fig. S10. Recycling HPLC profiles for separation of HF@C_{70} and H_2O@C_{70}.

fig. S11. ^{1}H NMR [151 MHz; $CDCl_3/CS_2$(1:1)] spectrum of the purified HF@C_{70}.

fig. S12. ^{13}C NMR [151 MHz; $CDCl_3/CS_2$ (1:1)] spectrum of the purified HF@C_{70}.

fig. S13. ^{1}H NMR [500 MHz; $CDCl_3/CS_2$ (1:1)] spectrum of the purified (H_2O·HF)@C_{70}.

fig. S14. ^{13}C NMR [151 MHz, $CDCl_3/CS_2$ (1:1)] spectrum of the purified (H_2O·HF)@C_{70}.

fig. S15. ^{19}F NMR [470 MHz; $CDCl_3/CS_2$ (1:1)] spectrum of the purified (H_2O·HF)@C_{70}.

fig. S16. APCI MS spectra (negative ionization mode) of $(HF)_2$@C_{70} and its theoretical isotopic patterns.

fig. S17. CV of (H_2O·HF)@C_{70} and empty C_{70} in ODCB with 0.1 M *n*-Bu_4NBF_4 at a scan rate of 20 mV s^{-1}.

fig. S18. UV-vis spectra of (H_2O·HF)@C_{70} and empty C_{70} in toluene.

fig. S19. IR reflection-absorption spectra on a gold substrate of empty C_{70}, HF@C_{70}, and (H_2O·HF)@C_{70}.

fig. S20. The calculated ^{1}H NMR for (H_2O·HF)@**α-13mem'** and (HF·H_2O)@**α-13mem'** obtained at the GIAO-B3LYP/6-311G(d,p)//M06-2X/6-31G(d).

fig. S21. The calculated ^{1}H and ^{13}C NMR for (H_2O·HF)@C_{70}, HF@C_{70}, and H_2O@C_{70}, at the GIAO-B3LYP/6-311G(d,p)//ONIOM-(MP2/6-311++G(3df,3pd):M06-2X/6-31G(d)).

fig. S22. X-ray structure of (H_2O·HF)@C_{70}.

table S1. Optimized geometry for (H_2O·HF)@**α-13mem'** at the M06-2X/6-31G(d).

table S2. Calculated ^{1}H and ^{13}C chemical shifts for (H_2O·HF)@**α-13mem'** obtained at the GIAO-B3LYP/6-311G(d,p)//M06-2X/6-31G(d).

table S3. Optimized geometry for (HF·H_2O)@**α-13mem'** at the M06-2X/6-31G(d).

table S4. Calculated ^{1}H and ^{13}C chemical shifts for (HF·H_2O)@**α-13mem'** obtained at the GIAO-B3LYP/6-311G(d,p)//M06-2X/6-31G(d).

table S5. Optimized geometry for (H_2O·HF)@**α-16mem'** at the M06-2X/6-31G(d).

table S6. Optimized geometry for (HF·H_2O)@**α-16mem'** at the M06-2X/6-31G(d).

table S7. Transition state for the positional exchange of the inner HF and H_2O inside **α-16mem'** at the M06-2X/6-31G(d).

table S8. Optimized geometry for HF@C_{70} at the ONIOM-(MP2/6-311++G(3df,3pd):M06-2X/6-31G(d)).

table S9. Calculated ^{1}H and ^{13}C chemical shifts for HF@C_{70} obtained at the GIAO-B3LYP/6-311G(d,p)//ONIOM-(MP2/6-311++G(3df,3pd):M06-2X/6-31G(d)).

table S10. Optimized geometry for (H_2O·HF)@C_{70} at the ONIOM-(MP2/6-311++G(3df,3pd):M06-2X/6-31G(d)).

table S11. Calculated ^{1}H and ^{13}C chemical shifts for (H_2O·HF)@C_{70} obtained at the GIAO-B3LYP/6-311G(d,p)//ONIOM-(MP2/6-311++G(3df,3pd):M06-2X/6-31G(d)).

table S12. Optimized geometry for HF at the M06-2X/6-31G(d).

table S13. Optimized geometry for HF at the MP2/6-311++G(3pd,3df).

table S14. Optimized geometry for HF dimer at the MP2/6-311++G(3pd,3df).

table S15. Optimized geometry for H_2O at the M06-2X/6-31G(d).

table S16. Optimized geometry for H_2O at the MP2/6-311++G(3pd,3df).

table S17. Optimized geometry for H_2O dimer at the MP2/6-311++G(3pd,3df).

table S18. Optimized geometry for H_2O·HF at the M06-2X/6-31G(d).

table S19. Optimized geometry for H_2O·HF at the MP2/6-311++G(3pd,3df).

table S20. Transition state for the proton exchange between HF and H_2O at the M06-2X/6-31G(d).

table S21. Transition state for the proton exchange between HF and H_2O at the MP2/6-311++G(3pd,3df).

table S22. Crystal data and structure refinement for (H_2O·HF)@C_{70}.

table S23. Atomic coordinates (×10^4) and equivalent isotropic displacement parameters (Å^2 × 10^3).

table S24. Bond lengths (Å) and angles (°).

table S25. Anisotropic displacement parameters (Å^2 × 10^3).

table S26. Hydrogen coordinates (× 10^4) and isotropic displacement parameters (Å^2 × 10^3).

table S27. Torsion angles (°).

References (*33*, *34*)

REFERENCES AND NOTES

1. K. R. Leopold, Hydrated acid clusters. *Annu. Rev. Phys. Chem.* **62**, 327–349 (2011).
2. S. M. Hurley, T. E. Dermota, D. P. Hydutsky, A. W. Castleman Jr., Dynamics of hydrogen bromide dissolution in the ground and excited states. *Science* **298**, 202–204 (2002).
3. A. Gutberlet, G. Schwaab, Ö. Birer, M. Masia, A. Kaczmarek, H. Forbert, M. Havenith, D. Marx, Aggregation-induced dissociation of HCl $(H_2O)_4$ below 1 K: The smallest droplet of acid. *Science* **324**, 1545–1548 (2009).
4. J.-W. Shin, N. I. Hammer, E. G. Diken, M. A. Johnson, R. S. Walters, T. D. Jaeger, M. A. Duncan, R. A. Christie, K. D. Jordan, Infrared signature of structures associated with the $H^+(H_2O)_n$ (n = 6 to 27) clusters. *Science* **304**, 1137–1140 (2004).
5. M. Miyazaki, A. Fujii, T. Ebata, N. Mikami, Infrared spectroscopic evidence for protonated water clusters forming nanoscale cages. *Science* **304**, 1134–1137 (2004).
6. D. Feller, K. A. Peterson, Hydrogen fluoride: A critical comparison of theoretical and experimental results. *J. Mol. Struct.:THEOCHEM* **400**, 69–92 (1997).
7. P. A. Giguère, S. Turrell, The nature of hydrofluoric acid. A spectroscopic study of the proton-transfer complex H_3O^+•F^-. *J. Am. Chem. Soc.* **102**, 5473–5477 (1980).

8. A. M. Elena, S. Meloni, G. Ciccotti, Equilibrium and rate constants, and reaction mechanism of the HF dissociations in the $HF(H_2O)_7$ cluster by ab initio rare event simulations. *J. Phys. Chem. A* **117**, 13039–13050 (2013).
9. D. F. Smith, Hydrogen fluoride polymer spectrum, hexamer and tetramer. *J. Phys. Chem.* **28**, 1040–1056 (1958).
10. S. Aoyagi, E. Nishibori, H. Sawa, K. Sugimoto, M. Takata, Y. Miyata, R. Kitaura, H. Shinohara, H. Okada, T. Sakai, Y. Ono, K. Kawachi, K. Yokoo, S. Ono, K. Omote, Y. Kasama, S. Ishikawa, T. Komuro, H. Tobita, A layered ionic crystal of polar Li@C_{60} superatoms. *Nat. Chem.* **2**, 678–683 (2010).
11. Z. Wang, S. Aoyagi, H. Omachi, R. Kitaura, H. Shinohara, Isolation and structure determination of a missing endohedral fullerene La@C_{70} through in situ trifluoromethylation. *Angew. Chem. Int. Ed.* **55**, 199–202 (2016).
12. A. A. Popov, S. Yang, L. Dunsch, Endohedral fullerenes. *Chem. Rev.* **113**, 5989–6113 (2013).
13. T. A. Murphy, T. Pawlik, A. Weidinger, M. Höhne, R. Alcala, J.-M. Spaeth, Observation of atomlike nitrogen in nitrogen-implanted solid C_{60}. *Phys. Rev. Lett.* **77**, 1075–1078 (1996).
14. S. Stevenson, in *Endohedral Fullerenes: From Fundamentals to Applications*, S. Yang, C. R. Wang, Eds. (World Scientific Publisihng Company, 2014), pp. 179–210.
15. G. C. Vougioukalakis, M. M. Roubelakis, M. Orfanopoulos, Open-cage fullerenes: Towards the construction of nanosized molecular containers. *Chem. Soc. Rev.* **39**, 817–844 (2010).
16. K. Komatsu, M. Murata, Y. Murata, Encapsulation of molecular hydrogen in fullerene C_{60} by organic synthesis. *Science* **307**, 238–240 (2005).
17. Y. Morinaka, F. Tanabe, M. Murata, Y. Murata, K. Komatsu, Rational synthesis, enrichment, and ^{13}C NMR spectra of endohedral C_{60} and C_{70} encapsulating a helium atom. *Chem. Commun.* **46**, 4532–4534 (2010).
18. K. Kurotobi, Y. Murata, A single molecule of water encapsulated in fullerene C_{60}. *Science* **333**, 613–616 (2011).
19. A. Krachmalnicoff, R. Bounds, S. Mamone, S. Alom, M. Concistrè, B. Meier, K. Kouřil, M. E. Light, M. R. Johnson, S. Rols, A. J. Horsewill, A. Shugai, U. Nagel, T. Rõõm, M. Carravetta, M. H. Levitt, R. J. Whitby, The dipolar endofullerene HF@C_{60}. *Nat. Chem.* **8**, 953–957 (2016).
20. A. Khong, H. A. Jiménez-Vázquez, M. Saunders, R. J. Cross, J. Laskin, T. Peres, C. Lifshitz, R. Strongin, A. B. Smith III, An NMR study of He_2 inside C_{70}. *J. Am. Chem. Soc.* **120**, 6380–6383 (1998).
21. Y. Morinaka, S. Sato, A. Wakamiya, H. Nikawa, N. Mizorogi, F. Tanabe, M. Murata, K. Komatsu, K. Furukawa, T. Kato, S. Nagase, T. Akasaka, Y. Murata, X-ray observation of a helium atom and placing a nitrogen atom inside He@C_{60} and He@C_{70}. *Nat. Commun.* **4**, 1554 (2013).
22. M. Murata, S. Maeda, Y. Morinaka, Y. Murata, K. Komatsu, Synthesis and reaction of fullerene C_{70} encapsulating two molecules of H_2. *J. Am. Chem. Soc.* **130**, 15800–15801 (2008).
23. R. Zhang, M. Murata, T. Aharen, A. Wakamiya, T. Shimoaka, T. Hasegawa, Y. Murata, Synthesis of a distinct water dimer inside fullerene C_{70}. *Nat. Chem.* **8**, 435–441 (2016).
24. R. Zhang, T. Futagoishi, M. Murata, A. Wakamiya, Y. Murata, Synthesis and structure of an open-cage thiafullerene $C_{69}S$: Reactivity difference of an open-cage C_{70} tetraketone relative to its C_{60} analogue. *J. Am. Chem. Soc.* **136**, 8193–8196 (2014).
25. A. Krachmalnicoff, R. Bounds, S. Mamone, M. H. Levitt, M. Carravetta, R. J. Whitby, Synthesis and characterisation of an open-cage fullerene encapsulating hydrogen fluoride. *Chem. Commun.* **51**, 4993–4996 (2015).
26. G. A. Olah, J. T. Welch, Y. D. Vankar, M. Nojima, I. Kerekes, J. A. Olah, Synthetic method and reactions. 63. Pyridinium poly(hydrogen fluoride) (30% pyridine-70% hydrogen fluoride): A convenient reagent for organic fluorination reactions. *J. Org. Chem.* **44**, 3872–3881 (1979).
27. L. Xu, H. Ren, S. Liang, J. Sun, Y. Liu, L. Gan, Release of the water molecule encapsulated inside an open-cage fullerene through hydrogen bonding mediated by hydrogen fluoride. *Chem. Eur. J.* **21**, 13539–13543 (2015).
28. J. S. Martin, F. Y. Fujiwara, High resolution nuclear magnetic resonance spectra of hydrogen fluoride in solution and in bihalide ions. Nuclear spin coupling in strong hydrogen bonds. *J. Am. Chem. Soc.* **96**, 7632–7637 (1974).
29. M. M. Olmstead, D. A. Costa, K. Maitra, B. C. Noll, S. L. Phillips, P. M. Van Calcar, A. L. Balch, Interaction of curved and flat molecular surfaces. The structures of crystalline compounds composed of fullerene (C_{60}, $C_{60}O$, C_{70}, and $C_{120}O$) and metal octaethylporphyrin units. *J. Am. Chem. Soc.* **121**, 7090–7097 (1999).
30. K. Masutani, S. Ochiai, in *Introduction to Experimental InfraredSpectroscopy: Fundamentals and Practical Methods*, M. Tasumi, Ed. (Wiley, 2015), pp. 141–152.
31. M. J. Frisch, G. W. Trucks, H. B. Schlegel, G. E. Scuseria, M. A. Robb, J. R. Cheeseman, G. Scalmani, V. Barone, B. Mennucci, G. A. Petersson, H. Nakatsuji, M. Caricato, X. Li, H. P. Hratchian, A. F. Izmaylov, J. Bloino, G. Zheng, J. L. Sonnenberg, M. Hada, M. Ehara, K. Toyota, R. Fukuda, J. Hasegawa, M. Ishida, T. Nakajima, Y. Honda, O. Kitao, H. Nakai, T. Vreven, J. A. Montgomery Jr., J. E. Peralta, F. Ogliaro, M. Bearpark, J. J. Heyd, E. Brothers, K. N. Kudin, V. N. Staroverov, T. Keith, R. Kobayashi, J. Normand, K. Raghavachari, A. Rendell, J. C. Burant, S. S. Iyengar, J. Tomasi, M. Cossi, N. Rega, J. M. Millam, M. Klene, J. E. Knox, J. B. Cross, V. Bakken, C. Adamo, J. Jaramillo, R. Gomperts, R. E. Stratmann, O. Yazyev, A. J. Austin, R. Cammi, C. Pomelli, J. W. Ochterski, R. L. Martin, K. Morokuma, V. G. Zakrzewski, G. A. Voth, P. Salvador, J. J. Dannenberg, S. Dapprich, A. D. Daniels, O. Farkas, J. B. Foresman, J. V. Ortiz, J. Cioslowski, D. J. Fox, in *Gaussian 09*, (Gaussian, Inc., 2013.
32. L. Chung, W. M. C. Sameera, R. Ramozzi, A. J. Page, M. Hatanaka, G. P. Petrova, T. V. Harris, X. Li, Z. Ke, F. Liu, H.-B. Li, L. Ding, K. Morokuma, The ONIOM method and its applications. *Chem. Rev.* **115**, 5678–5796 (2015).
33. V. Schettino, M. Pagliai, G. Cardini, The infrared and Raman spectra of fullerene C_{70}. DFT calculation and correlation with C_{60}. *J. Phys. Chem. A* **106**, 1815–1823 (2002).
34. G. M. Sheldrick, *SHELX-97*, *Program for the Refinement of Crystal Structures* (University of Göttingen, 1997).

Acknowledgments

Funding: Financial support was provided by the Japan Society for the Promotion of Science KAKENHI Grant Numbers JP23241032, JP15K13641, JP15H0093, JP15H00939, and JP15J09612. The NMR measurements were supported by the Joint Usage/Research Center at the Institute for Chemical Research, Kyoto University. **Author contributions:** Y.M. conceived and designed the projects. R.Z. performed most of the experimental works and theoretical calculations and wrote the paper, supported by M.M. and A.W. The IR measurements were performed by T.S. and T.H. **Competing interests:** The authors declare that they have no competing interests. **Data and materials availability:** All data needed to evaluate the conclusions in the paper are present in the paper and/or the Supplementary Materials. Additional data available related to this paper may be requested from the authors. Metrical parameters for the structure of (H_2O·HF) @C_{70} is available free of charge from the Cambridge Crystallographic Data Center under reference number CCDC-1513130.

Submitted 15 November 2016
Accepted 11 February 2017
Published 21 April 2017
10.1126/sciadv.1602833

Citation: R. Zhang, M. Murata, A. Wakamiya, T. Shimoaka, T. Hasegawa, Y. Murata, Isolation of the simplest hydrated acid. *Sci. Adv.* **3**, e1602833 (2017).

ScienceAdvances
AAAS

Isolation of the simplest hydrated acid
Rui Zhang, Michihisa Murata, Atsushi Wakamiya, Takafumi Shimoaka, Takeshi Hasegawa and Yasujiro Murata (April 21, 2017)
Sci Adv 2017, 3:.
doi: 10.1126/sciadv.1602833